

**Multi-model assessment of anthropogenic influence
on record global and regional warmth during 2015**

Jonghun Kam^{1,2}, Thomas R. Knutson¹, Fanrong Zeng¹, and Andrew T. Wittenberg¹

To be submitted to BAMS (special supplement on Explaining Extreme Events of 2015)

September 16, 2016

¹ NOAA/Geophysical Fluid Dynamics Laboratory, Princeton, New Jersey

² Cooperative Institute for Climate Science, Princeton University, Princeton, New Jersey

Summary

In 2015, record warm surface temperatures were observed for the global mean, India, and the equatorial central Pacific. CMIP5 simulations suggest that for the global mean and India cases, anthropogenic warming were largely to blame.

Introduction

HadCRUT4v4 observed surface temperature data (Morice et al. 2012; 5°x5° lat.-lon. gridbox) indicates that 2015 was a clear record-breaking year for global annual-mean temperatures (Figure 1 a and b). In this analysis, we consider only grid-boxes with at least 100 years of historical data, which narrows the focus mainly to the Atlantic and Indian Oceans, North Pacific Ocean, Europe, the U.S., southern Asia and Australia (Fig. 1c). 16% of this analyzed area experienced record annual warmth during 2015 (Figure 1d).

Relative to the 1881-1920 mean, observed global temperatures had over the past decade been warming at a rate less than the ensemble-mean warming in the Coupled Model Inter-comparison Project phase 5 All-Forcing historical runs (CMIP5-ALL; Taylor et al. 2012). However, the record global temperature of 2015 (Figure 1 e), including the influence of a strong El Niño event (Figure 1 f), was nearly as warm globally as the mean of the CMIP5-ALL model ensemble levels for 2015.

Major regions with unprecedented annual-mean warmth in 2015 included the northeast Pacific and northwest Atlantic, while during September-November (SON) 2015, Southern India/Sri Lanka stood out with record seasonal warmth (Fig. 1 g)¹. Only a small region south of Greenland (0.2% of the globe) experienced record annual-mean cold surface temperatures (Figure 1 d).

Based on Fig. 1d, we constructed our regions of focus. These regions had some irregular shapes and were constructed to be mostly covered by new record annual or seasonal temperatures in 2015, with the two main regions of focus (aside from the global mean) being the Niño4 region (annual means) and a region including southern India and Sri Lanka (September-November means). To demonstrate the robustness for annual-mean record warmth in 2015 over the Niño4 region (Fig. 1g), we also showed extended Reconstructed Sea Surface Temperature (ERSST v4; Huang et al. 2016) and Hadley Centre Sea Ice and Sea Surface Temperature (HadISST v1.1; Rayner et al. 2003) data reconstructions and found that these also show unprecedented annual-mean warmth during 2015.

This study investigates the causes of these record warm events using an 8-model set of all-forcing (anthropogenic + natural) historical climate model runs, associated long-term control (unforced) runs, and natural forcing runs (CMIP5–ALL, –CONT, and –NAT). These eight models (listed in Supplementary Material) were selected as they were the only ones with NAT simulations extending to 2012. Our methods follow the studies of Knutson et al. (2013 and 2014); some of the descriptive text below is drawn from those reports.

Time-evolving trend analyses for long-term global and regional anthropogenic warming

¹ Our region of focus in southern India and Sri Lanka does include some SST influence, as we used the combined SST/Tair dataset (see Supplementary Material).

Fig. 2 (a-c) shows analyses for long-term global and regional trends using different start years, but with a common end year (2012 for CMIP5–NAT and 2015 for CMIP5–ALL; the latter are extended with simulations forced by the RCP4.5 emissions scenario). Observed trends ending in 2012 and 2015 are shown for comparison. For the sliding trends, we require at least 33% areal coverage in the region for the start year of the trend (Knutson et al., 2013), resulting in the gaps shown. The global-mean analysis shows a pronounced observed warming, consistent with CMIP5–ALL yet statistically distinct from CMIP5–NAT, for all start years before about 1990. While the CMIP5–ALL runs appear inconsistent with observed global trends through 2012 (at least for recent trends beginning in the 1990s), now that the record has been extended to 2015, we find that CMIP5–ALL trends beginning in the late 1990s now overlap the observations.

For the Niño4 region (Figure 2 b), we compare results from three different observational data sets. The ERSSTv4 shows the strongest indication of a detectable warming, consistent with the CMIP5–ALL runs but inconsistent with the CMIP5–NAT runs for start years up to around 1960. In contrast, the HadISSTv1.1 estimated trends are hardly distinguishable from the CMIP5–NAT runs, and also inconsistent with the CMIP5–All runs through most of the period. The observed seasonal-mean time series (SON) over Southern India/Sri Lanka (Figure 2c) shows a pronounced warming, consistent with CMIP5–ALL regardless of trend start year, and detectable relative to CMIP5–NAT for start years up to the 1970s.

Overall, the trend analysis using the CMIP5 models shows a long-term warming over the globe and Southern India/Sri Lanka (very likely attributable in part to anthropogenic forcing), and long-term trend results for the Niño4 region that strongly depend on observational data uncertainties.

Model-based attributable risk assessment for the 2015 extreme warm anomalies

Considering the anomalies and new record-breaking temperatures in 2015, there are many regions that could have been selected for the fraction of attributable risk (FAR; Stott et al. 2004) analysis. The major regions of records include global, eastern Pacific, western Atlantic, Indian Ocean, Europe, and south of Greenland (cold record). For our report, we chose to compute the FAR for global temperature, the NINO4 region (with the prominent El Niño in 2015), and southern India/Sri Lanka (Sept.-November). The FAR compares the event tail probabilities (P) between the CMIP5–NAT and CMIP5–ALL runs ($\text{FAR} = 1 - P_{\text{nat}}/P_{\text{all}}$). Forced responses are derived from the multi-model ensemble means of the CMIP5–ALL and CMIP5–NAT simulations, while the impact of internal variability on the modeled trend distributions was estimated using the CMIP5–CONT runs (Knutson et al. 2013). Our FAR estimates use the first- (2015) and second-ranked observed positive anomaly as the extreme event thresholds (Fig. 2d). For extremely high anomalies, the FAR can be particularly difficult to estimate, as it is based on a ratio of very small areas under distribution tails (Kam et al. 2015). Therefore we used the second-ranked observed anomalies as the threshold values for our FAR estimates, as these anomalies are not quite as extreme as the top-ranked ones.

According to the HadCRUT4v4, the second-ranked anomalies over the globe, Southern India/Sri Lanka, and the Niño4 region occurred in 2014, 2010, and 1888, respectively, while the ERSSTv4 and HadISST v1.1 datasets show the second-ranked anomalies over the Niño4 region occurred in different years, (2002 and 1987, respectively). Based on the HadCRUT4v4, the simulated probabilities of exceeding the second-ranked anomalies for the globe, Southern India/Sri Lanka, and the Niño4 region are 58% (0.005%), 23% (0.3%), 32% (1.5%) for the CMIP5–ALL (CMIP5–NAT) runs, respectively. Sensitivity tests for the Niño4 region using the

second-ranked anomalies from the ERSST v.4 and HadISST v.1.1 datasets are consistent with the results from the HadCRUT4v4 (not shown). The FAR estimates are 0.99, 0.98, and 0.95, for the globe, Southern India/Sri Lanka (SON), and the Niño4 regions, respectively. Uncertainties in the FAR estimates were explored by computing the spread of FAR estimates across individual CMIP5 models (Fig. 2g). These sensitivity tests show that, using the second-ranked year threshold values, the estimated FAR is above 0.9 for seven, five, and five out of eight individual models for the globe, Niño4 region, and Southern India/Sri Lanka, respectively.

A crucial assumption of our study is that the internal variability simulated by the models represents the real-world variability adequately. The modeled variability is used as the null hypothesis for explaining trends, and if it is underestimated (overestimated) this makes it too easy (difficult) to detect significant trends and too difficult (easy) for model simulations to be consistent with observations (Knutson et al. 2013). Therefore, we evaluated the decadal variability of temperature anomalies over the Niño4 region by comparing a derived observed variability with CMIP5 control run variability. Variability comparisons for other regions have been previously summarized in Knutson et al. (2013), and plots similar to Fig. 2e for global temperature and the southern India/Sri Lanka region are shown in Supplemental Material.

To isolate the decadal variability, we apply a low-pass filter with a half-power point at nine years. For the observed internal variability temperature estimate, we subtracted the grand ensemble mean of the CMIP5–ALL runs from observations to attempt to remove the forced component of the observed variations. We have not adjusted the forced component estimate to better fit the observations as done in Mann et al. (2014) and Steinmann et al. (2015), which would be a further refinement beyond the scope of this study. As a sensitivity test for Niño4, we compared the modeled variability (8 GCMs shown in Fig. 2h and 23 GCMs in Supplementary

Materials) with that estimated from three different observational datasets. To estimate the model internal variability, we compute the temperature anomaly variance using each model's entire control run. Details for these calculations, and control run lengths used, are described in Knutson et al. (2013). The 8 GCM control runs show a wide range of the simulated decadal variances, between 0.025 and 0.08 °C². The analogous estimates of the unforced component of the variance from the observational reanalyses are 0.048 °C² (ERSSTv4) and 0.051 °C² (HadCRUT4v4), both of which are located near the center of the inter-model histogram of the control run decadal variances, while the HadISSTv1.1 shows a somewhat larger decadal variance (0.068 °C²) which is greater than that from five of the eight models. The sensitivity tests for observed decadal variances, and our earlier sliding trend analyses, indicate that for the Niño4 region, observational uncertainties significantly obscure the detection and attribution of past trends or recent extreme events.

Conclusions

For 2015, the tendency for a greater ratio of global area covered by extreme annual-mean warm vs. cold events, as seen in recent decades, has continued. According to the CMIP5 models, the *risk* of events exceeding the extreme (1st or 2nd-ranked) thresholds for the globe, the Niño4 region, and Southern India/Sri Lanka is almost entirely attributable to anthropogenic forcing, with the ensemble-mean FAR above 0.9, and with strong agreement regarding relatively high FAR estimates among the eight GCMs that provided natural-forcing simulations. The strongest model-based evidence for detectable long-term anthropogenic warming, and the highest confidence in a large fraction of attributable risk, was found for the global mean and Southern India/Sri Lanka (SON). In the Niño4 region, confidence in long-term trend assessment and in the

142 FAR estimates is limited, due to uncertainties in the observational data and a wide range of
143 simulated decadal variances from the control runs.

144

145 **Acknowledgements** We thank the WCRP's Working Group on Coupled Modeling, participating
146 CMIP5 modeling groups, for making available the CMIP5. This study was partly funded by
147 NOAA grant NA14OAR4320106.

1 *References.*

- 2 Huang, B., V.F. Banzon, E. Freeman, J. Lawrimore, W. Liu, T.C. Peterson, T.M. Smith, P.W.
3 Thorne, S.D. Woodruff, and H.-M. Zhang, 2014, Extended Reconstructed Sea Surface
4 Temperature version 4 (ERSST.v4): Part I. Upgrades and intercomparisons. *J. Climate*, **28**,
5 911-930.
- 6 Kam, J., T. R. Knutson, F. Zeng, and A. T. Wittenberg, 2015, Record annual-mean warmth over
7 Europe, the northeast Pacific, and the northwest Atlantic during 2014: Assessment of
8 anthropogenic influence, [in "Explaining extreme events of 2014 from a climate
9 perspective"], *Bull. Amer. Meteor. Soc.*, **96**, S61-S65.
- 10 Knutson, T. R., F. Zeng, and A. T. Wittenberg, 2013: Multimodel assessment of regional surface
11 temperature trends: CMIP3 and CMIP5 Twentieth Century simulations. *J. Climate*, **26**,
12 8709–8743.
- 13 Knutson, T. R., F. Zeng, and A. T. Wittenberg, 2014: Multimodel assessment of extreme annual-
14 mean warm anomalies during 2013 over regions of Australia and the western tropical Pacific.
15 [in “Explaining Extreme Events of 2013 from a Climate Perspective”]. *Bull. Amer. Meteor.*
16 *Soc.*, **95**, S26–S30.
- 17 Mann, M. E., B. A. Steinman, and S. K. Miller, 2014: On forced temperature changes, internal
18 variability, and the AMO. *Geophys. Res. Lett.*, **41**, 3211–3219, doi: 10.1002/2014GL059233,
19 <http://dx.doi.org/10.1002/2014GL059233>.
- 20 Morice, C. P., J. J. Kennedy, N. A. Rayner, and P. D. Jones, 2012: Quantifying uncertainties in
21 global and regional temperature change using an ensemble of observational estimates: The
22 HadCRUT4 data set. *J. Geophys. Res.*, **117**, D08101, doi:10.1029/2011JD017187.
- 23 Steinman, B. A., M. E. Mann, and S. K. Miller, 2015: Atlantic and Pacific multidecadal
24 oscillations and northern hemisphere temperatures. *Science*, **347**, 988–991.
- 25 Stott, P. A., D. A. Stone, and M. R. Allen, 2004, Human contribution to the European heatwave
26 of 2003, *Nature*, **432**, 610-614.
- 27 Taylor, K. E., R. J. Stouffer, and G. A. Meehl, 2012: An overview of CMIP5 and the
28 experimental design. *Bull. Amer. Meteor. Soc.*, **93**, 485–498.
- 29 Rayner, N. A.; Parker, D. E.; Horton, E. B.; Folland, C. K.; Alexander, L. V.; Rowell, D. P.;
30 Kent, E. C.; Kaplan, A., 2003, Global analyses of sea surface temperature, sea ice, and night
31 marine air temperature since the late nineteenth century, *J. Geophys. Res.*, **108**, 4407.

List of Figure Captions

Figure 1: a-b) Annual time series of the fractions of available global area with the top three warmest (red curve) and coldest (blue curve) in the available record to that date (a) and to the entire record through 2015 (b). c) Annual mean surface air temperature anomalies ($^{\circ}\text{C}$) for 2015 (relative to the 1961-90 base period) from the HadCRUT4 data set. d) Colors identify grid boxes with annual mean anomalies that rank 1st (dark red), 2nd (orange-red), or 3rd (yellow-orange) warmest in the available observed record. Only colored and gray areas have sufficiently long records, defined here as containing at least 100 available annual means, which require at least four available months. e-g) Annual-mean surface temperature anomalies ($^{\circ}\text{C}$) for the globe, Niño4 region, and Southern India/Sri Lanka (SON). Red (CMIP5-ALL) and blue (CMIP5-NAT) curves indicate ensemble-mean simulated anomalies through 2015 and 2012, respectively, with each available model weighted equally; orange curves indicate individual CMIP5-ALL ensemble members. Black curves indicate observed estimates from HadCRUT4v4 (solid) and NOAA NCDC (dotted); All time series are adjusted to have zero mean over the period 1881-1920. For the Niño4 region, alternative observed anomalies from the ERSSTv4 and HadISSTv1.1 reconstructions and the ensemble anomalies for CMIP5-ALL are shown with $+2.5^{\circ}\text{C}$ and -2.5°C offsets from zero for display purposes.

Figure 2: a-c) Sliding trends as a function of starting year, with ending year 2015 (black solid line) or 2012 (black dashed line) ($^{\circ}\text{C}/100\text{ yr}$) for the globe, the Niño4 region, and Southern India/Sri Lanka. Black, red, and blue curves depict observations, CMIP5-ALL ensemble mean, and CMIP5-NAT ensemble mean, respectively. Red (blue) lines depict the mean of trends from the CMIP5-ALL (CMIP5-NAT) runs, while pink (blue) bands depict the 5th-95th percentile range for an individual realization chosen randomly from the simulations, with equal representation for each model. Purple shading indicates the overlap of the pink and blue region. d) Estimates of the FAR of exceeding the first (2015) and second-ranked observed temperature anomaly thresholds from the CMIP5 multi-model ensemble (large red and orange circle, respectively); black solid circles correspond to the FAR estimated from the eight paired CMIP5-ALL and -NAT runs from individual CMIP5 models, for the second-ranked observed anomalies. e) Histogram of the Niño4 region variances for non-overlapping 155-year epochs of the eight individual model control runs, along with estimates from three observational datasets from which the model-estimated forced response has been removed (1861-2015).

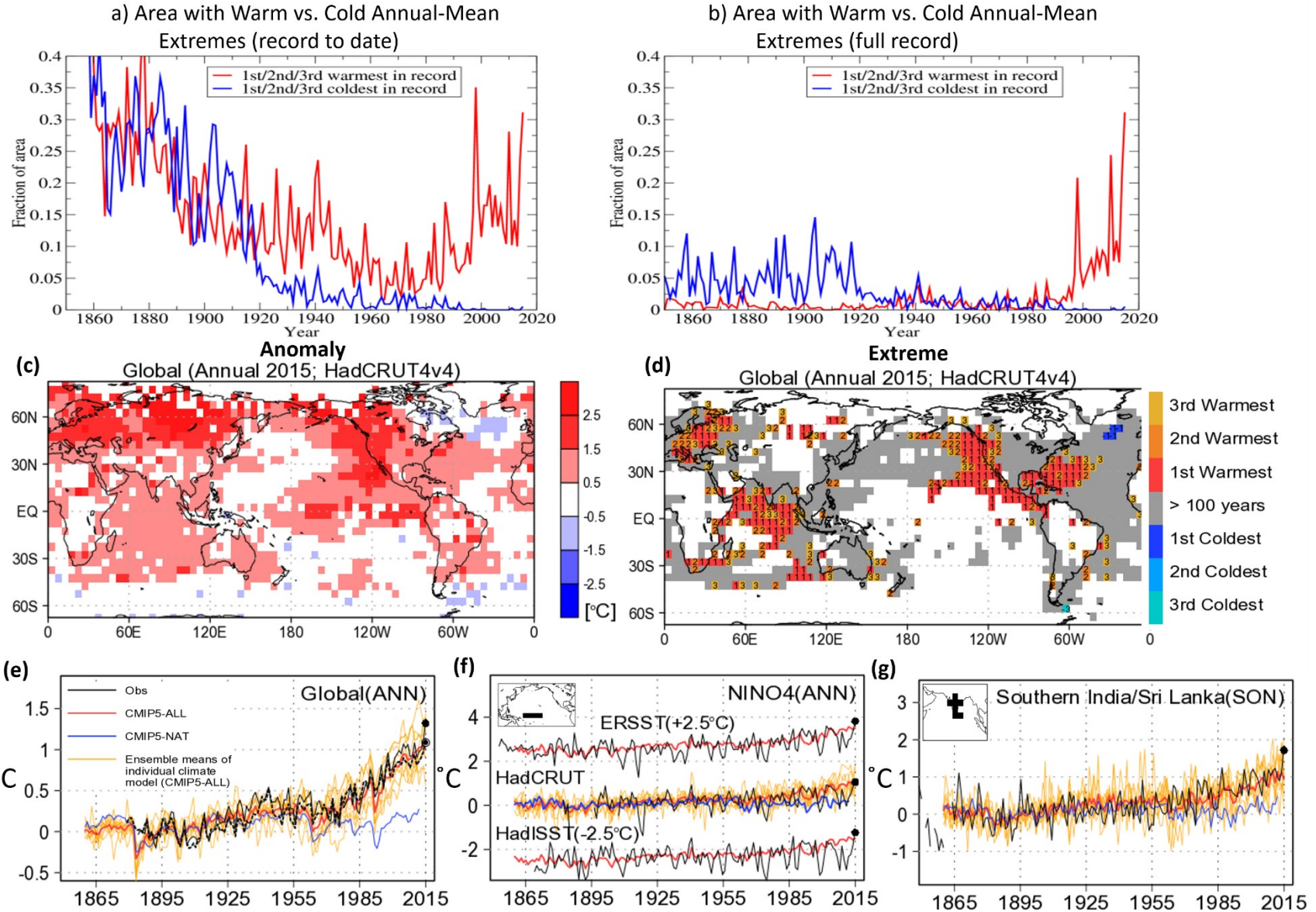


Figure 1.

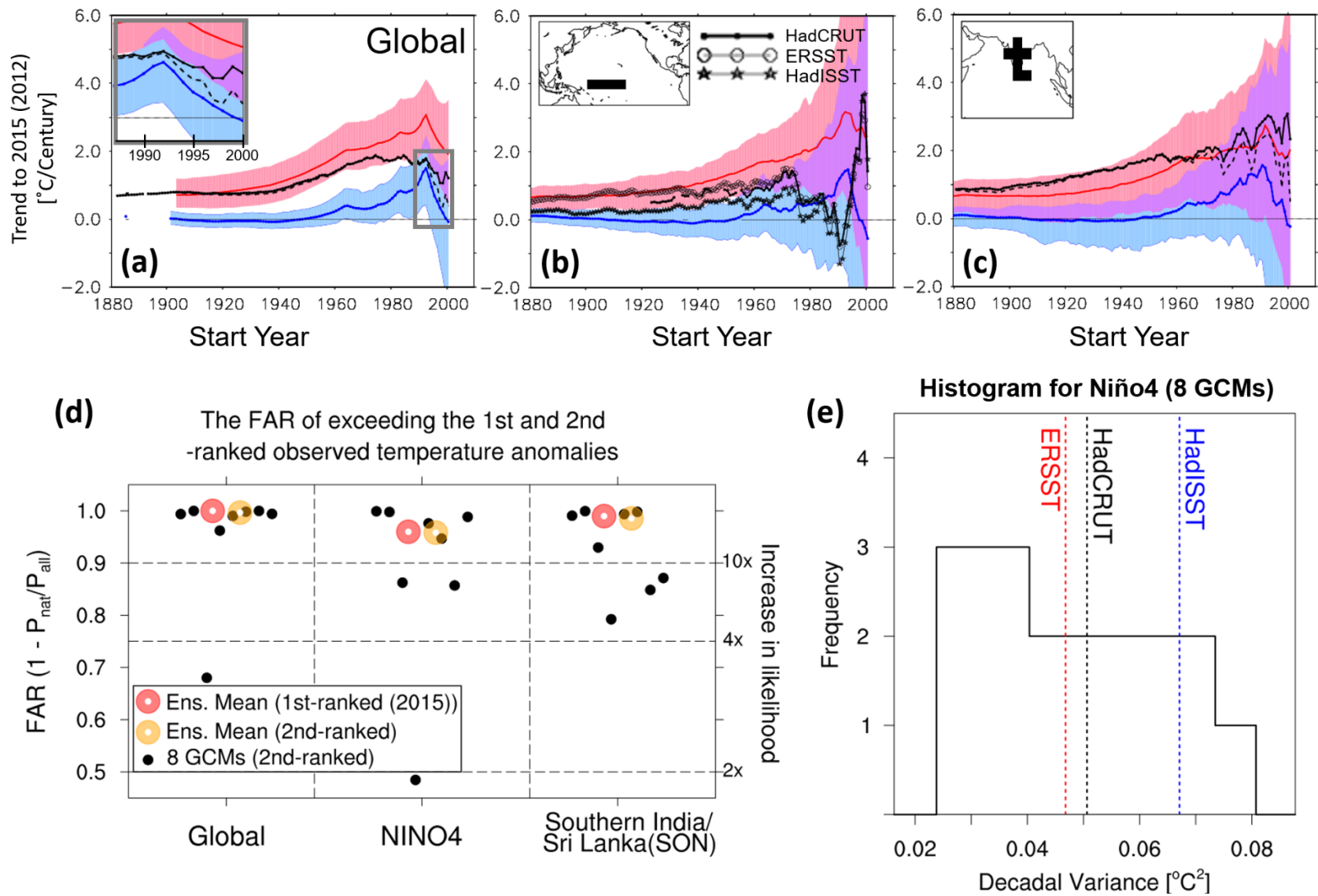


Figure 2.